

A novel class of potential prion drugs: preliminary *in vitro* and *in vivo* data for multilayer coated gold nanoparticles†

Hoang Ngoc Ai Tran,^{‡a} Fernanda Sousa,^{‡§b} Fabio Moda,^{‡c} Subhra Mandal,^d Munish Chanana,^{¶e} Chiara Vimercati,^c Michela Morbin,^c Silke Krol,^{§b} Fabrizio Tagliavini^c and Giuseppe Legname^{*af}

Received 30th July 2010, Accepted 2nd September 2010

DOI: 10.1039/c0nr00551g

Gold nanoparticles coated with oppositely charged polyelectrolytes, such as polyallylamine hydrochloride and polystyrenesulfonate, were examined for potential inhibition of prion protein aggregation and prion (PrP^{Sc}) conversion and replication. Different coatings, finishing with a positive or negative layer, were tested, and different numbers of layers were investigated for their ability to interact and reduce the accumulation of PrP^{Sc} in scrapie prion infected ScGT1 and ScN2a cells. The particles efficiently hampered the accumulation of PrP^{Sc} in ScN2a cells and showed curing effects on ScGT1 cells with a nanoparticle concentration in the picomolar range. Finally, incubation periods of prion-infected mice treated with nanomolar concentrations of gold nanoparticles were significantly longer compared to untreated controls.

Introduction

Prion diseases are fatal and incurable neurodegenerative disorders of animals and humans.¹ They can manifest as genetic, infectious and sporadic illnesses and they include bovine spongiform encephalopathy of cattle, scrapie of sheep, chronic wasting disease of deer, moose and elk, Creutzfeldt–Jakob and Gerstmann, Sträussler and Scheinker diseases of humans.² The molecular mechanism of prion diseases consists in the conformational conversion of the cellular, membrane-anchored host prion protein (PrP^C), into an altered pathogenic isoform, denoted PrP^{Sc}, through a conversion of the α -helix structures into β -sheets.³

Prion replication involves the direct interaction between the PrP^{Sc} template and the endogenous cellular PrP^C driving the formation of nascent infectious prions.⁴ Molecules binding to either PrP^C or PrP^{Sc} conformers at the binding interface may inhibit this interaction, thus interrupting prion production.

Additionally, compounds that bind molecules supporting and participating in prion replication, such as chaperones or other ligands, may also be good candidates for blocking prion replication.

Many compounds have been proposed for the treatment of prion diseases, including polysulfated anions, dextrans, and cyclic tetrapyrroles.^{5–8} Recently, some success has been achieved using pentosanpolysulfate⁹ although this compound seems to be unsuccessful in the treatment of human prion diseases.¹⁰

In addition, molecules targeting the different molecular steps involved in pathological prion replication have also been investigated.^{11–17} Treatment of cells with Fab fragments has been proved effective in clearing pre-existing PrP^{Sc}.¹⁵ However, to date, the use of these compounds in clinical applications is limited, due to their high toxicity and poor crossing of the blood–brain barrier (BBB). Thus, there is an urgent need to develop systematic pharmacological and mechanistic studies for the identification of a new class of compounds as therapeutic agents capable of inhibiting several pathways in prion conversion and replication.

The field of nanoparticle technology is rapidly expanding and promises revolutionary advances in the diagnosis and treatment of many devastating human diseases. Nanoparticles have been developed to allow targeted delivery and sustained release of therapeutics. Such nanoparticle-based drug formulations interact with biological systems both at molecular and supra-molecular levels. Nanoparticles can be tailored to respond to specific cell environments, and even to induce desired physiological responses in cells, whilst minimizing unwanted side effects. Compared to conventional drugs, nanoparticles-bearing therapeutics possess higher intrinsic pharmacological activity and their main advantage is their small dosage that would not require the administration of large amounts of potentially toxic therapeutics.¹⁸

Here, we report the preparation of coated gold nanoparticles (AuNPs) exposing, on their surface, functional groups that can selectively bind, inhibit or prevent the formation of misfolded protein

^aLaboratory of Prion Biology, Neurobiology Sector, Scuola Internazionale Superiore di Studi Avanzati (SISSA), Ed. Q1, Basovizza Campus, S.S.14 Km. 163,5, 34149 Trieste, Italy. E-mail: legname@sissa.it; Fax: +39 040 3756 502; Tel: +39 040 3756 515

^bNanoBioMed Laboratory@LANADA, CBM—Cluster in Biomedicine, Area Science Park, Basovizza, Trieste, Italy

^cDivision of Neurology and Neuropathology, Carlo Besta Neurological Institute, Milan, Italy

^dSISSA, via Bonomea 265, Trieste, Italy. E-mail: mandal@sissa.it

^eMax-Planck Institute of Colloids and Interfaces, Wissenschaftspark Golm, Am Mühlenberg 1, Potsdam, Germany

^fELETTRA Laboratory, Sincrotrone Trieste S.C.p.A., Area Science Park, Basovizza, Trieste, Italy

† Electronic supplementary information (ESI) available: HRTEM image of a 2A coated nanogold particle; Western blot of cell lysate from ScGT1 cells treated with nanoparticles (a) 2A, (b) 2A-46 nm, (c) 5S, and (d) 5S-46 nm. See DOI: 10.1039/c0nr00551g

‡ These authors contributed equally to the work.

§ Present address: European Center of Nanomedicine, Neurological Institute “Carlo Besta”, Milan, Italy.

¶ Present address: Departamento de Química Física, Universidade de Vigo, Campus Universitario, Vigo, Spain.

aggregates such as prions. The build-up of nanoparticles was carried out with gold nanoparticles as core and a layer-wise deposition of oppositely charged polyelectrolytes, such as polycation polyallylamine hydrochloride (PAH) and polyanion polystyrenesulfonate (PSS). To examine the structure–activity relationship, we tested different numbers of layers, as well as the nanoparticles' outermost layer surface charge, for their possible role in inhibiting scrapie prion formation *in vitro* and *in vivo*. Our findings represent the first report of functionalized nanoparticles as novel potent anti-prion drugs.

Results

Physical characteristics of polyelectrolyte-multilayer coated gold nanoparticles

The physical characteristics of the coated nanoparticles are given in Table 1. For the experiments to inhibit PrP^{Sc} replication *in vitro*, particles from 1 to 5 layers were prepared, finishing with either a positive (PAH) or negative (PSS) charged layer. All particle preparations finishing with PSS were tagged as *nS* ($n = 1–5$) and each one with PAH was labeled *mA* ($m = 1–5$). The layers were deposited onto AuNPs with a hydrodynamic diameter (D_h) of 19.9 ± 0.2 nm *via* an electrostatic driven self-assembly process and their size was measured by dynamic light scattering (DLS). DLS usually gives a larger diameter than electron microscopy, because it also measures the ionic shell (citrate) around the hard core (gold). As an example, in Fig. S1 (ESI†) we show a high-resolution transmission electron microscopy (HRTEM) image of a coated (2A) AuNP. As can be noted, the particle is around 15 nm in diameter and, in the dehydrated form in ultra-high vacuum, the 2 layers of the coating measures less than 1 nm. The thickness is not perfectly homogenous, but the coating is covering the particle surface completely.

The concentration was determined *via* UV-VIS absorption spectrometry. It has to be noted that with UV-VIS it was only possible to quantify the AuNPs concentration but not the concentration of the active compounds which are the

polyelectrolyte. Experiments are under development to quantify directly the polycation and polyanion concentration on the surface. Table 1 shows that the particle diameter increases with every deposited layer. In addition, the successful deposition of the polyelectrolyte layers was confirmed by the change in surface charge (ζ -potential measurements).

Finally, experiments were performed to investigate if the curvature of the AuNPs had an effect on functionality. To this purpose, AuNPs with a bigger diameter (45.7 ± 0.3 nm) were prepared and tested.

Anti-prion potency and cytotoxicity of nanoparticles in cell lines

Potency of known drugs such as quinacrine and imipramine was used as a control²⁰ for anti-prion activity in our cell models, two different types of immortalized neuronal cells, GT1 and N2a. The potency of quinacrine and imipramine was similar to previous publications,²¹ as indicated in Table 2; namely EC_{50} of quinacrine was 0.4 ± 0.1 and 0.3 ± 0.1 μ M for ScGT1 and ScN2a, respectively; whereas for imipramine EC_{50} was 6.2 ± 0.4 and 5.5 ± 0.5 μ M for ScGT1 and ScN2a, respectively. In comparison, citrate stabilized AuNPs without polyelectrolyte layers did not show any detectable prion inhibitory activity.

The number of layers and the surface charge of the nanoparticles influenced survival of the neuronal cells, ScGT1 and ScN2a. Cytotoxicity was determined by measuring the number of cells surviving after incubation in the drug-doped medium for 5 days, assayed with calcein-AM in a fluorescence plate reader. With positively charged particles (1–5A) a 92–100% cell viability was obtained and with negatively charged particles (1–5S) the 74–100% of the cells survived (Table 2).

Moreover, the concentration at which complete inhibition of PrP^{Sc} formation in ScGT1 and ScN2a cells is achieved was determined by immunoblotting. Particle preparations were added at different concentrations to scrapie-infected cells, and the inhibitory activity was measured over 5 days. PrP^{Sc} levels were quantified by ELISA. The resulting EC_{50} of the particles with a positive outermost layer (*mA*) was in the range of 8.3 ± 0.5 to 25.4 ± 1.3 pM in ScGT1 and 8.4 ± 0.6 to 30.0 ± 1.4 pM in ScN2a cells (Table 2). In both cases, the influence of size and number of layers on efficacy was limited. However, prion inhibition by particles with a negative outermost layer (*nS*) showed an increase in efficacy with a higher number of layers. In particular, EC_{50} of 1S was 121.4 ± 6.5 pM and 5S was 35.0 ± 1.4 pM in ScGT1 while EC_{50} of 1S was 248.7 ± 12.9 pM and 5S was 129.9 ± 7.1 pM in ScN2a cells (Table 2).

To investigate the influence of particle curvature on prion inhibition, bigger AuNPs were used. Regarding the AuNPs with a diameter of 46 nm, efficacy and cytotoxicity were only tested for 2A and 5S coatings. Both tested cell types showed cell viability in the range of 90–100% (Table 2). Prion inhibition of 2A-46 nm was similar to 2A, and 5S-46 nm was 3 times less effective than 5S (Fig. S2† and Table 2).

Coated gold nanoparticles uptake studies

The uptake mechanism of AuNPs coated with 2A or 5S was monitored in the two different types of immortalized neuronal cells used in this study, GT1 and N2a. Fig. 1 shows the uptake of

Table 1 Physical characteristics of the nanoparticles

Nanoparticles	D_h /nm	ζ -potential/mV	Concentration/ nm	Number of particles/mL
	Mean \pm SD	Mean \pm SD		
NG-15 nm	19.9 ± 0.2	-40.0 ± 0.4	33.0	1.99×10^{13}
1A ^a	105.1 ± 2.9	52.8 ± 0.9	18.7	1.12×10^{13}
2A	128.9 ± 9.9	63.0 ± 0.9	30.3	1.83×10^{13}
3A	112.3 ± 6.3	58.8 ± 0.9	32.7	1.97×10^{13}
4A	110.9 ± 3.2	65.4 ± 5.4	14.2	8.55×10^{13}
5A	110.1 ± 1.4	56.4 ± 3.2	14.2	8.55×10^{13}
1S ^a	59.0 ± 1.7	-50.7 ± 1.3	37.9	2.28×10^{13}
2S	88.7 ± 5.4	-48.1 ± 3.8	29.2	1.76×10^{13}
3S	103.8 ± 0.6	-56.0 ± 3.3	24.5	1.48×10^{13}
4S	98.6 ± 5.0	-49.8 ± 6.1	16.1	9.72×10^{13}
5S	94.0 ± 0.7	-53.6 ± 0.5	14.2	8.55×10^{13}
NG-46 nm	45.7 ± 0.3	-32.4 ± 3.2	82.9	4.99×10^{13}
2A	86.9 ± 1.8	50.8 ± 0.8	61.3	7.38×10^{12}
5S	155.4 ± 8.3	-39.6 ± 0.83	34.0	4.10×10^{12}

^a A—outermost layer PAH and S—outermost layer PSS. The mean particle size (D_h) and zeta-potential (ζ -potential) were obtained from cumulative measurements (SD, $n = 6$).

Table 2 PrP^{Sc} inhibition and cellular toxicity of quinacrine, imipramine and the nanoparticles in ScGT1 and ScN2a cells

Compounds Small molecules	PrP ^{Sc} inhibition ^a		% Cell viability \pm SE ^b	
	ScGT1 (EC ₅₀ \pm SE/ μ M)	ScN2a (EC ₅₀ \pm SE/ μ M)	ScGT1	ScN2a
Quinacrine	0.4 \pm 0.1	0.3 \pm 0.1	100 \pm 4	100 \pm 2
Imipramine	6.2 \pm 0.4	5.5 \pm 0.5	100 \pm 7	100 \pm 5

^a EC₅₀—compound concentration required to reduce PrP^{Sc} level 50% *versus* untreated cells. ^b Cell viability at EC₅₀ values was determined by calcein-AM cytotoxicity assay and expressed as an average percent of viable cells *versus* control untreated cells (SE, *n* = 3).

Nanoparticles	ScGT1 (EC ₅₀ \pm SE/pM)	ScN2a (EC ₅₀ \pm SE/pM)	ScGT1	ScN2a
Positive surface charge—PAH (NG-15 nm)				
1A	8.3 \pm 0.5	8.4 \pm 0.6	100 \pm 6	100 \pm 3
2A	8.8 \pm 0.2	24.5 \pm 1.0	100 \pm 1	97 \pm 1
3A	10.1 \pm 0.2	20.4 \pm 0.5	100 \pm 7	96 \pm 3
4A	25.4 \pm 1.3	25.1 \pm 1.2	100 \pm 6	100 \pm 5
5A	20.1 \pm 1.1	30.0 \pm 1.4	100 \pm 3	92 \pm 1
Negative surface charge—PSS (NG-15 nm)				
1S	121.4 \pm 6.5	248.7 \pm 12.9	95 \pm 2	92 \pm 5
2S	99.8 \pm 4.7	220.3 \pm 11.8	97 \pm 1	87 \pm 3
3S	70.1 \pm 3.2	149.5 \pm 6.1	74 \pm 7	90 \pm 3
4S	50.3 \pm 2.0	130.1 \pm 5.4	100 \pm 2	90 \pm 7
5S	35.0 \pm 1.4	129.9 \pm 7.1	84 \pm 8	93 \pm 4
NG-46 nm				
2A	10.3 \pm 0.3	30.2 \pm 1.7	100 \pm 4	94 \pm 2
5S	89.7 \pm 3.5	329.5 \pm 10.7	90 \pm 1	91 \pm 6

5S nanoparticles by GT1 (Fig. 1a and b) and N2a cells (Fig. 1c) at 2 and 24 h. This was deduced by co-localization of two fluorescent dyes evident from the yellow signal due to the overlap of the red fluorescence emitted by lipid dye DiA, incorporated in the membrane encircling the nanoparticles, and the green fluorescence from FITC-PAH bound to AuNP (Fig. 1a, arrow in 7th image). In contrast if the particles are only attached to the plasma membrane the fluorescence is green (Fig. 1a, ring in 3rd image). Images were acquired 2 hours after incubation of GT1 cells with the coated AuNPs.

After 24 h GT1 cells still show the yellow signal of nanoparticles in vesicles (Fig. 1b). The same uptake mechanism was observed for N2a cells (Fig. 1c) imaged 2 h after incubation with particles.

In vitro effect of the nanoparticles on prion fibril formation

Given 2A and 5S potent anti-prion activity in scrapie-infected cells, these two particles were chosen to test their ability in inhibiting recombinant PrP fibril formation in an amyloid seeding assay (ASA).²² Using full-length recombinant mouse (Mo) PrP(23–230) as template and ScN2a- and ScGT1-PTA precipitated prions as seeds in a standard ASA assay, 2A and 5S, at concentrations of 50 pM and 200 pM, respectively, extended the lag phase by 5–15 hours, hence showing a much slower kinetics than the control (Fig. 2). The potency of 2A and 5S in delaying PrP fibril formation suggests that these nanoparticles may directly interact with PrP and prevent its conversion into the pathogenic PrP^{Sc}-like form. In light of these results, ASA could also be utilized to study the mechanistic steps involved in the

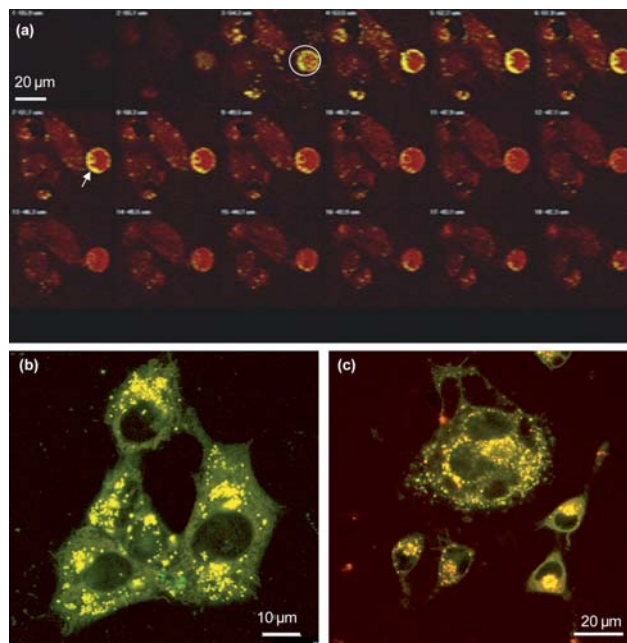


Fig. 1 Uptake of coated nanoparticles into immortalized neuronal cells. The particles were labeled with FITC (green) and cell membranes were stained with DiA (red). Co-localization of particles in vesicles gave a yellow signal. (a) 3D optical sectioning of GT1 cells incubated for 2 h with 5S coated nanogold. The white circles in section 3 indicate coated gold nanoparticles attached to the cell surface and therefore showing only green fluorescence. The arrow in section 7 indicates membrane encircled structures filled with nanoparticles (yellow). (b) 5S nanoparticles in GT1 cells after 24 hours of incubation. (c) 5S nanoparticles in N2a cells after 2 hours of incubation.

inhibitory effects of drugs screened for prion diseases, and of AuNPs in particular.

In vivo application of the nanoparticles

Outbred CD-1 mice were intracerebrally inoculated with 30 μ L of 10% RML brain homogenates, pre-incubated with a nanomolar concentration of gold nanoparticles 2A or 5S. Before the inoculation, TEM analysis of nanoparticle-treated homogenates confirmed the presence of sparsely distributed particles. The incubation period of mice treated with both 2A (mean \pm standard error of the mean SEM: 139 \pm 3 days) and 5S (mean \pm SEM: 135 \pm 2 days) was significantly longer (respectively $p = 0.0021$ and $p = 0.023$, log-rank test) than that of control animals infected with pure RML homogenate (mean \pm SEM: 128 \pm 2 days) (Fig. 3a). Only 2A-treated animals showed a modest, but statistically significant, increase of survival time compared with controls (163 \pm 3 vs. 152 \pm 3 days and $p = 0.025$, log-rank test), whereas treatment with nanoparticles 5S was not as effective (151 \pm 1 vs. 152 \pm 3 days and $p = 0.075$, log-rank test) (Fig. 3b). Histopathological assessment of haematoxylin and eosin (H&E)-stained sections was carried out on all mice brains

(Fig. 3c). Neuropathological results showed similar moderate spongiform alterations in each group of mice, with a major involvement of the hippocampus (Fig. 3d–f), thalamus (Fig. 3g–i) and somatosensory cortex.

For PrP^{res} biochemical analysis (Fig. 4) brain homogenates were treated with proteinase K (PK), analyzed by SDS-PAGE and Western blotting, using anti-PrP monoclonal antibody 6H4. Immunohistochemistry showed similar PrP^{res} immunoreactivity in the form of synaptic and diffuse deposits in the cerebral cortex, basal ganglia, hypothalamus, hippocampus, brainstem, cerebellum, and thalamus (Fig. 4b–d), which was often affected by coarse PrP^{res} deposition (Fig. 4e–g). Glial immunoreaction (GFAP) was mainly detected in the hippocampus, thalamus, mesencephalic nuclei, brainstem and the granular layer of the cerebellar cortex. To summarize, all immunohistochemical analysis (6H4, GFAP, and CNPase) did not underline any difference between groups of mice challenged with different inocula. Kidneys, spleens and livers of mice inoculated with both RML and mock nanoparticles-treated homogenates were analyzed, and indicated the lack of acute systemic toxicity following the injection of the particles. Even the brains of mice inoculated with mock pre-incubated with nanoparticles 2A or 5S did not reveal specific alterations correlated to a potential toxic effect of the particles on the CNS. These results were also confirmed by periodical MRI analysis (data not shown). Immunoblot analysis of brain homogenates revealed the same PrP^{Sc} profile for all groups of mice (Fig. 4a).

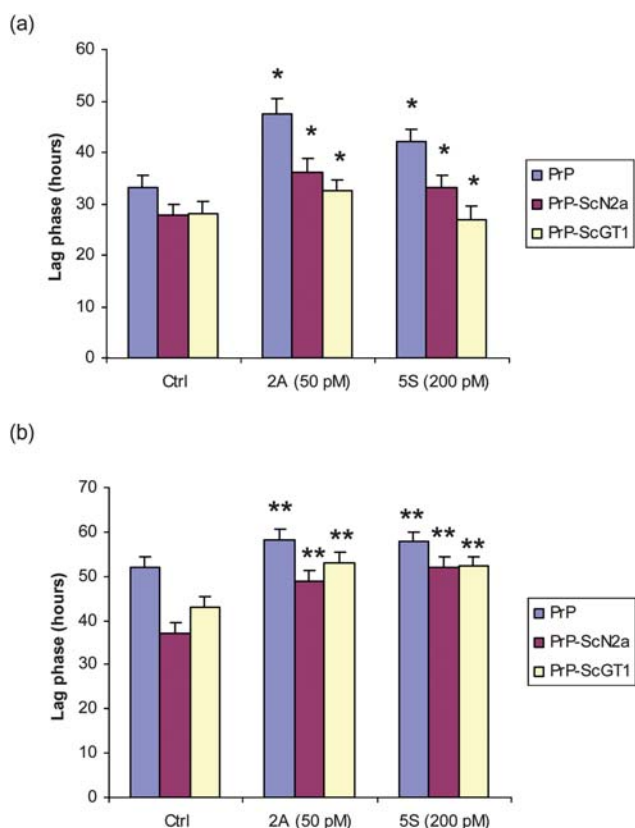


Fig. 2 Effect of the nanoparticles on fibril formation and ASA. Lag phase of amyloid-formation kinetics is compared between (a) SpectraMax M5 and (b) Gemini EM instruments (Molecular Devices) in the assays, using full-length MoPrP(23–230) and amyloid seeding with ScN2a- and ScGT1-PTA precipitated protein in the presence of coated gold nanoparticles. 50 pM of 2A nanoparticles or 200 pM of 5S nanoparticles were added to each well. The Student's *t*-test (two-tailed) was used to determine significant differences among measurements ($n = 4$). * $P < 0.05$ and ** $P < 0.01$.

Discussion

Due to their intrinsic properties as being non-toxic, inert to most chemical reactions, coupled with easy and fast preparation, pure AuNPs are excellent candidates for use in both therapeutic²³ and diagnostic approaches. Citrate-stabilized AuNPs maintain good long-term stability in solution. Gold nanoparticles can be functionalized using Layer-by-Layer (LbL) deposition.^{24,25} Polyelectrolyte assembling on AuNPs is induced by electrostatic interactions between the oppositely charged polyelectrolytes. A supersaturated concentration of the polyelectrolytes was chosen for the LbL, in order to guarantee fast and complete surface coverage and good stability.²³

The range for the number of deposited layers was chosen to present the precursor region described by Decher as model for the deposition of a strong and weak polyelectrolyte.²⁶ The first five to eight layers of deposited polyelectrolytes differ from the following set of layers in terms of composition and thickness, and are called precursor layers. The attractive and repulsive forces of the underlying layers as well as that of the core contribute to the self-assembly of the polyelectrolyte. If the core is negatively charged, the first positively charged polyelectrolyte layer will be self-assembled exclusively by attractive forces, and by binding they will overcompensate the charge of the core. For the next layer, the opposite charge of the first polyelectrolyte layer is present, but due to the vicinity to the core also the repulsive forces by the like-wise charged core. This leads to a less tight binding and a decreased amount of bound polyelectrolytes. Moreover, the polyelectrolyte layers penetrate each other in the precursor layer, and are thinner than the following set of layers, which are more distant from the core.²⁶ We used the intercalation

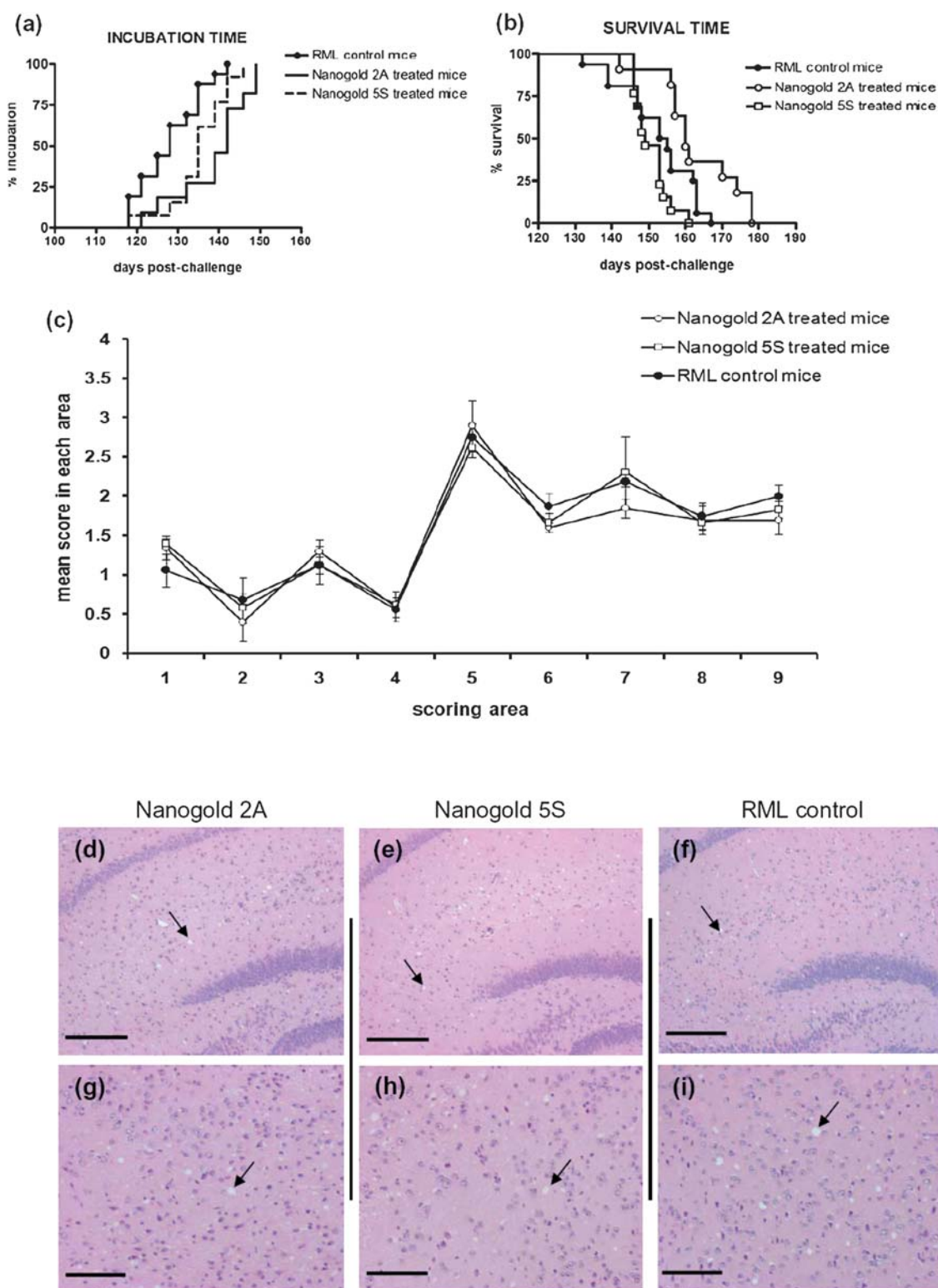


Fig. 3 Incubation time, survival curves and vacuolation profile. Coated gold 2A and 5S nanoparticles were able to delay the incubation period of RML infected mice if compared with untreated controls (a), while only nanoparticles 2A-treated animals showed a moderate but statistically significant increase in survival time compared with controls, whereas treatment with nanoparticles 5S was not effective (b). Vacuolation profile (c) was scored on a scale of 0–5 in the following brain areas: (1) dorsal medulla, (2) cerebellar cortex, (3) superior culliculus, (4) hypothalamus, (5) thalamus, (6) hippocampus, (7) septum, (8) retrosplenial and adjacent motor cortex, and (9) cingulated and adjacent motor cortex. Data are mean \pm SEM. Micrographs were obtained from areas of hippocampal and thalamic regions (most affected by vacuolation) stained with haematoxylin–eosin (d–i). Spongiosis in mice inoculated with RML brain homogenates pre-incubated with nanogold 2A (d and g) or 5S (e and h), and untreated (f and i) are shown. Scale bar: 200 μ m (d–f) and 100 μ m (g–i).

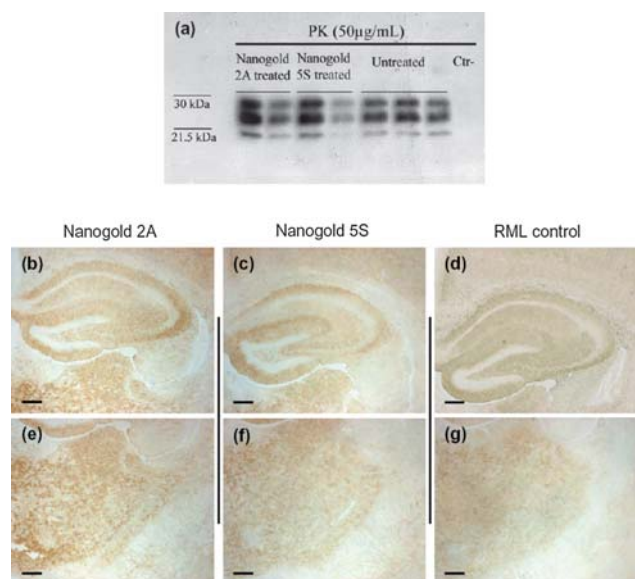


Fig. 4 PrP^{res} immunohistochemical and biochemical analysis. Western blot analysis of PK-resistant mouse PrP. Immunoblot data revealed the same PrP^{Sc} profile in all groups of mice (a), while immunohistochemical results showed the same synaptic-diffuse pattern of PrP^{Sc} deposition for each group of mice (b–g). Micrographs were obtained from areas of hippocampus (b–d) and thalamus (e–g). Pyramidal cells layer and dentate gyrus of the hippocampus were spared from PrP^{res} accumulation. Synaptic and coarse PrP^{res} immunostaining was detected into the thalamus of every group of mice. Scale bar: 200 μ m.

of polycations and polyanions, containing either sulfonate or primary amine groups, to selectively bind and inhibit prion formation, creating a surface exposing both moieties randomly and in varying ratios.

There is some reported evidence that polyamines can have an effect on PrP^{Sc}. Indeed, Supattapone and co-workers²⁷ found that branched polyamines are able to disintegrate aggregates of PrP^{Sc} to undetectable levels. For polysulfates, the influence of their chemical structure on selective binding to either PrP^C or PrP^{Sc} leading to prion inhibitory activity was also demonstrated.²⁸ In our work, both functional groups were combined on the surface of the AuNPs in varying ratios, to obtain a platform of possible interactive sites for the misfolded PrP.

Two studies on the bio-distribution of citrate stabilized AuNPs should also be considered, though the results were somehow contradictory: De Jong and co-workers²⁹ found that only 10 nm particles were crossing the BBB, while Sonavane and co-workers³⁰ found 50 nm particles in the brain. Our particles were found to have a hydrodynamic diameter 90 to 130 nm, and in electron microscopy the fully dehydrated polyelectrolyte matrix was condensed until it was only 1–2 nm thick. We assume that the polyelectrolyte shell loses some of its water molecules while crossing the BBB.

From previous experiments on cells of the BBB, it is known that AuNPs coated with different numbers of polyelectrolyte layers are cytotoxic (for example, porcine brain capillary endothelial cells).²⁴ Moreover, a strong dependency on the number of layers and surface charge was observed. Polycations were more cytotoxic than polyanions and with lower number of layers more cytotoxic than a higher number of layers. An additional binding

of albumin to the final polyelectrolyte layer should diminish the toxicity, and animal experiments confirmed that after intracranial inoculation no toxicity leading to morphological changes in the brain was present (Sousa *et al.*, unpublished data).

Preliminary *in vivo* experiments showed the efficacy of both nanoparticles (2A and 5S) to interfere with prion propagation. Because of the limited information available about the toxic effects of these particles when injected in animals, we started our experiments by using a dosage of compound lower than those generally reported in the literature for other therapeutic approaches.²⁹ Whereas 5S nanoparticles significantly increased only the incubation time of treated mice, 2A nanoparticles showed higher anti-prion activity. Indeed, even when 2A were used at nanomolar concentrations (25.35 nM), a moderate but statistically significant increase in both incubation and survival time was observed, thus indicating a possible interaction between PrP^{Sc} and the nanoparticles. Even though the animals were treated with just a single dose of nanoparticles the increase of incubation and survival time were statistically significant. Several studies are currently underway to determine the best 2A concentration, able to inhibit or perhaps completely block disease progression. To this end, several mice were intracerebrally infected with RML brain homogenate pre-incubated with higher dosages of 2A particles (53 nM vs. 25.35 nM). Groups of control mice were also included to monitor the onset of general toxic effects. Since the gold 2A, modified with the addition of albumin in the outermost layer, were able to cross BBB (Sousa *et al.*, unpublished data), new therapeutic approaches based on their injection into the tail vein of mice have already been scheduled.

Experimental

Synthesis of gold nanoparticles

Monodisperse AuNPs were prepared as described by Turkevich *et al.*²² For particles with a size of 15 ± 1 nm, 5.3 mg of NaAuCl₄·2H₂O in 25 mL of Milli-Q grade water were boiled under reflux. One millilitre of a 1% trisodium citrate solution was rapidly added to the boiling pale yellow solution, which resulted in a color change to deep red. After boiling for additional 20 min, the solution was cooled down to room temperature and stored protected from light at room temperature. All experiments described here were performed with the above colloidal gold nanoparticle stock solution.

The 46 nm gold particles were prepared using the same procedure but with 10.6 mg of NaAuCl₄ in 25 mL water and the fast addition of 750 μ L 1% trisodium citrate solution.

Polyelectrolyte coating

The polyelectrolyte coating was applied in accordance to the method previously described with a few modifications.^{23–25} Briefly, 1 mL colloidal AuNPs was added drop-wise under constant stirring to 200 μ L of PSS solution (10 mg mL⁻¹) or 500 μ L PAH solution (3 mg mL⁻¹). Both solutions are supersaturated to allow for an immediate coverage of the particles with polyelectrolytes. After incubation for 20 min in the dark, this solution was centrifuged for 20 min at $20\,000 \times g$. The supernatant was removed and the particles were washed twice by

centrifugation/resuspension in Milli-Q water. Prior to the next layer deposition the coated AuNPs were stored in the dark for 1 hour. The coated particles were then incubated with the oppositely charged polyelectrolyte. Each coating step was proved on an NS Zetasizer (Malvern, Milan, Italy) with dynamic light scattering (DLS) for size and polydispersity index (PDI) and ζ -potential measurements for changes in the surface charge. The concentration of the AuNPs was determined at 580 nm in a UV/Vis spectrometer applying the Beer–Lambert law ($\lambda_{\text{abs}} = 518$ nm and $\epsilon = 5.14 \times 10^7 \text{ M}^{-1} \text{ cm}^{-1}$).¹⁹

Transmission electron microscopy of coated gold nanoparticles

High-resolution transmission electron microscopy (HRTEM) measurements were performed by diluting the coated AuNP solution with Milli-Q water to a ratio of 1 : 100. Then the solution was deposited on a carbon-covered 200 mesh copper grid and dried in air at room temperature. The images were acquired with acceleration voltage ranging from 18.5 to 150 kV. The non-digital images were digitized and the data analyses of the images were performed using ImageJ software.

Cell culture, drug treatment and cell viability

Cell culture, drug treatment and cell viability were performed in accordance to the protocols described previously.^{31,32}

PrP^{Sc}/PrP^{res} detection by Western blot

After 5 days of drug treatment, the accumulation of PrP^{Sc} was detected by proteinase K (PK) digestion followed by immunoblotting of lysed cells as described previously.¹⁵ Mouse brain homogenates from frozen tissues (10% (w/v)) were prepared and an equivalent to 100 μg was digested with 50 $\mu\text{g mL}^{-1}$ of PK for 1 hour at 37 °C. Reactions were terminated by the addition of 5 mM phenylmethanesulfonyl fluoride. Treated homogenates were loaded on 12.5% polyacrylamide gels, transferred to PVDF membranes and probed with anti-PrP antibody 6H4 (1 : 10 000, Prionics) and anti-CNPase antibody (1 : 1000, Sigma Aldrich). The immunoreactions were visualized by enhanced chemiluminescence system (Amersham). The quantification of PrP^{Sc} by ELISA followed a protocol described previously.³³

Detection of *in vitro* effect of the nanoparticles on prion fibril formation and amyloid seeding assay (ASA)

Fibril formation was performed in accordance to the method previously described with a few modifications.²¹ Briefly, 500 μL of 2 mg mL^{-1} ScN2a or ScGT1 cell lysates were used for PTA precipitation by adding 500 μL of PBS/4% sarkosyl/protease inhibitor and 0.5% PTA with continuous shaking at 37 °C, 350 rpm for 1 hour, and centrifuged at room temperature, 14 000 $\times g$ for 30 min. The pellets were washed with 500 μL of PBS/2% sarkosyl/protease inhibitor, centrifuged and resuspended in 150 μL of water and then stored at -80 °C until use. In ASA, 4 μL of resuspended PTA pellets were diluted into 400 μL of water and 20 μL of the diluted sample were added to each well containing 180 μL of reaction solution (50 $\mu\text{g mL}^{-1}$ MoPrP(23–230), 0.4 M GdnHCl, and 10 μM ThT in 1 \times PBS buffer) in a 96-well black plate (BD Falcon). The nanoparticles were added in different

concentrations to each well. Each sample was performed in four replicates. Each well contained one 3 mm glass bead (Sigma). The plate was covered with sealing tape (Fisher Scientific), incubated at 37 °C with continuous shaking and read on a SpectraMax M5 or Gemini EM fluorescence plate reader (Molecular Devices) by top fluorescence reading every 5 min at excitation of 444 nm and emission of 485 nm.

Preparation of gold nanoparticles pre-treated brain homogenates

10% RML (Rocky Mountain Laboratories) infected brain homogenate (wt/vol) was prepared from pools of brains of terminally RML-sick CD-1® IGS mice (Charles River Laboratories), while 10% mock homogenate (wt/vol) was obtained from pools of brains of healthy CD-1 mice. 2A and 5S coated AuNPs were separately pre-incubated with both RML and mock brain homogenates at 4 °C for 24 hours. Even RML and mock brain homogenates untreated with nanoparticles were subjected at the same pre-treatment. The final 2A coated AuNPs concentration in both RML and mock homogenates was 25.35 nM while that of AuNPs 5S was 26.65 nM.

Analysis of the homogenates by transmission electron microscopy

Mouse brain homogenates (both RML and mock) treated with 2A or 5S particles were dissolved in distilled water (1 : 2) then 5 μL of the final suspension were applied to Formvar-carbon-200 mesh nickel grids for 6', negatively stained with uranyl acetate and observed with an electron microscope (EM109 Zeiss, Oberkochen, Germany) operated at 80 kV at a standard magnification ($\times 30$ 000), calibrated with an appropriate grid. The samples were evaluated for the presence and amount of AuNP aggregates.

Animal inoculation

All mice were divided into six different groups, housed in ventilated cages and identified by ear-tags. Each group was intracerebrally inoculated with 30 μL of a precise solution: *i.e.* (i) RML or (ii) mock brain homogenate pre-incubated with AuNPs 2A; (iii) RML or (iv) mock brain homogenate pre-incubated with AuNPs 5S; (v) RML and (vi) mock brain homogenates untreated. 10–15 mice for each group were anesthetized with sevoflurane and inoculated into the right caudatus nucleus by using Hamilton syringes with 26 G needle. Both preparations of the inocula and their injection were carried out using sterile instrumentation and disposable equipment for each animal and each inoculum. Groups of mock-inoculated and untreated mice were included as controls.

Behavioral monitoring

Behavioral monitoring was carried out weekly, beginning at 16 weeks post-inoculation, and included spontaneous locomotor activity in the open field, nest construction test, reactivity to external stimuli and inverted screen test.^{34,35} The incubation time was calculated as the period between the day of inoculation and the appearance of clinical signs of disease, confirmed by a subsequent assessment at 3 days interval. At the terminal stage of disease (characterized by ataxia, hunched dorsal kyphosis, and

suppressed righting reflex) clinically affected mice were sacrificed, while the other mice were monitored for the entire predicted life span and then culled and subjected to necropsy.

Histological examinations

All mouse tissues were collected for the study. Regarding CNS, the left hemisphere of each mouse brain was fixed in Carnoy solution at 4 °C for 24 hours,³⁶ while the right hemisphere was frozen at -80 °C for Western blot analysis. The same procedure was followed for the other organs (*i.e.* brainstem, muscle, spleen, liver, kidney, Peyer's patch, *etc.*). Fixed brain samples were cut in four standard coronal levels,³⁷ dehydrated, and embedded in paraplast. 7 µm thick serial sections from paraffin embedded tissues were stained with hematoxylin–eosin (HE) or probed with different antibodies (*i.e.* 6H4, GFAP, Caspase-3, *etc.*). Spongiform profiles were determined on HE-stained sections, by scoring the vacuolar changes in nine standard grey matter area as described.³⁷

Immunohistochemical staining

Sections were immunostained with monoclonal antibody to PrP (6H4 1 : 1000, Prionics), monoclonal antibody to myelin protein (CNPase 1 : 500, Sigma Aldrich), polyclonal antibody to glial fibrillary acidic protein (GFAP 1 : 1000, Dako), monoclonal antibody to T-lymphocyte (CD3ε, 1 : 500, Millipore) and a polyclonal antibody to apoptotic cells (Caspase-3 1 : 100, Millipore). Before PrP immunostaining, the sections were sequentially subjected to PK digestion (10 µg mL⁻¹, room temperature, 5') and guanidine isothiocyanate treatment (3 M, room temperature, 20'), and non-specific binding was prevented using Animal Research Kit Peroxidase (Dako). Immunoreactions were visualized using 3-3'-diaminobenzidine (DAB, Dako) chromogen.

Proteinase K (PK) immunoblot analysis

10% (wt/vol) brain homogenates from frozen tissues were prepared in lysis buffer (100 mM sodium chloride, 10 mM EDTA, 0.5% Nonidet P40, and 0.5% sodium deoxycholate in 10 mM Tris–HCl, pH 7.4). Aliquots of cleared lysate equivalent to 100 µg were digested with 50 µg mL⁻¹ of PK for 1 h at 37 °C. Reactions were terminated by the addition of phenylmethanesulfonyl fluoride (PMSF, 5 mM). Treated homogenates were loaded on 12.5% polyacrylamide gels, transferred to polyvinylidene fluoride membranes and probed with anti-PrP antibody 6H4 (1 : 10 000, Prionics), anti-CNPase antibody (1 : 1000, Sigma Aldrich) and anti-Caspase-3 antibody (1 : 100, Millipore). The immunoreactions were visualized by enhanced chemiluminescence system (Amersham).

Magnetic resonance imaging (MRI)

Magnetic resonance imaging was performed in clinically symptomatic CD-1 mice challenged with RML and in non-infected control mice on a Bruker BioSpec 70/30 USR Tesla scanner. Mice were anesthetized with isoflurane at a dose approximately of 2.5 L min⁻¹, modulated according to the breathing frequency. The animals were positioned on apposite bed inside the magnet

and were monitored throughout the procedure for breathing frequency and body temperature with specific probes. Twenty-six axial slices were acquired for each mouse with T2 High Resolution Turbo Spin Echo sequences. The following parameters were employed: thickness 0.60 mm without gap, TR 3000 ms, TE 27.1 ms, FOV 2.20/2.20 cm, and 256 matrix.

Statistical analysis

Statistical analyses were performed using the GraphPad-Prism 4.0 software. Kaplan–Meier survival curves were plotted, and differences in survival between groups of mice inoculated with RML (positive control) and RML pre-incubated with AuNPs 2A or AuNPs 5S were compared using the log-rank test.

Conclusions

The polyelectrolyte multilayer-coated gold nanoparticles are a novel class of potential anti-prion drugs. While they showed *in vitro* very high efficacy at very low concentration, their potential *in vivo* to inhibit completely prion aggregation needs further improvement. A slight increase in inoculation time and survival time was observed for the 2A coated particles and at the tested concentration. Further concentrations as well as other coatings need to be studied *in vivo* as the correlation between the *in vitro* experiments and the *in vivo* inoculation is not so striking. Especially the extremely low concentration required to suppress complete the prion aggregation raises the expectations that this small amount of particles will pass the blood–brain barrier and will enter the brain parenchyma.

Acknowledgements

This work has been supported by grants from the Compagnia di San Paolo and Italian Ministry of Health to GL, by financial support of the Italian government through a CIPE grant to FS and SK, and by Italian Ministry of Health and Associazione Italiana Encefalopatie da Prioni to FT. The authors wish to thank I. Campagnani and M. Ruggerone for monitoring and care of the experimental animals and G. Furlan for editing and proofreading the manuscript.

References

- 1 S. B. Prusiner, *Proc. Natl. Acad. Sci. U. S. A.*, 1998, **95**, 13363.
- 2 S. B. Prusiner and K. K. Hsiao, *Ann. Neurol.*, 1994, **35**, 385.
- 3 K. M. Pan, M. Baldwin, J. Nguyen, M. Gasset, A. Serban and D. Groth, et al., *Proc. Natl. Acad. Sci. U. S. A.*, 1993, **90**, 10962.
- 4 S. B. Prusiner, M. R. Scott, S. J. DeArmond and F. E. Cohen, *Cell*, 1998, **93**, 337.
- 5 R. H. Kimberlin and C. A. Walker, *Arch. Virol.*, 1983, **78**, 9.
- 6 B. Ehlers and H. Diringer, *J. Gen. Virol.*, 1984, **65**, 1325.
- 7 H. Diringer and B. Ehlers, *J. Gen. Virol.*, 1991, **72**, 457.
- 8 S. A. Priola, A. Raines and W. S. Caughey, *Science*, 2000, **287**, 1503.
- 9 K. Doh-ura, K. Ishikawa, I. Murakami-Kubo, K. Sasaki, S. Mohri and R. Race, et al., *J. Virol.*, 2004, **78**, 4999.
- 10 Y. Tsuboi, K. Doh-ura and T. Yamada, *Neuropathology*, 2009, **29**, 632.
- 11 B. Caughey and R. E. Race, *J. Neurochem.*, 1992, **59**, 768.
- 12 P. Meier, N. Genoud, M. Prinz, M. Maissen, T. Rüllicke and A. Zurbriggen, et al., *Cell*, 2003, **113**, 49.
- 13 A. Rhie, L. Kirby, N. Sayer, R. Wellesley, P. Disterer and I. Sylvester, et al., *J. Biol. Chem.*, 2003, **278**, 39697.

-
- 14 D. Proske, S. Gilch, F. Wopfner, H. M. Schätzl, E. L. Winnacker and M. Famulok, *ChemBioChem*, 2002, **3**, 717.
 - 15 D. Peretz, R. A. Williamson, K. Kaneko, J. Vergara, E. Leclerc and G. Schmitt-Ulms, et al., *Nature*, 2001, **412**, 739.
 - 16 M. Horiuchi, G. S. Baron, L. W. Xiong and B. Caughey, *J. Biol. Chem.*, 2001, **276**, 15489.
 - 17 V. Perrier, A. C. Wallace, K. Kaneko, J. Safar, S. B. Prusiner and F. E. Cohen, *Proc. Natl. Acad. Sci. U. S. A.*, 2000, **97**, 6073.
 - 18 S. K. Sahoo and V. Labhsetwar, *Drug Discovery Today*, 2003, **8**, 1112.
 - 19 X. Liu, M. Atwater, J. Wang and Q. Huo, *Colloids Surf., B*, 2007, **58**, 3.
 - 20 C. Korth, B. C. H. May, F. E. Cohen and S. B. Prusiner, *Proc. Natl. Acad. Sci. U. S. A.*, 2001, **98**, 9836.
 - 21 D. W. Colby, Q. Zhang, S. Wang, D. Groth, G. Legname and D. Riesner, et al., *Proc. Natl. Acad. Sci. U. S. A.*, 2007, **104**, 20914.
 - 22 J. Turkevich, P. C. Stevenson and J. Hillier, *Discuss. Faraday Soc.*, 1951, **11**, 55.
 - 23 G. Schneider and G. Decher, *Langmuir*, 2008, **24**, 1778.
 - 24 M. Chanana, A. Gliozzi, A. Diaspro, I. Chodnevskaja, S. Huewel and V. Moskalenko, et al., *Nano Lett.*, 2005, **5**, 2605.
 - 25 G. Schneider and G. Decher, *Nano Lett.*, 2004, **4**, 1833.
 - 26 G. Decher, in *Multilayer thin films*, ed. G. Decher and J. Schlenoff, Wiley-VCH, Weinheim, 2003, pp. 1–17.
 - 27 S. Supattapone, H. Wille, L. Uyechi, J. Safar, P. Tremblay and F. C. Szoka, et al., *J. Virol.*, 2001, **75**, 3453.
 - 28 R. Trevitt and J. Collinge, *Brain*, 2006, **129**, 2241.
 - 29 W. H. De Jong, W. I. Hagens, P. Krystek, C. Burger Marina, A. J. A. M. Sips and R. E. Geertsma, *Biomaterials*, 2008, **29**, 1912.
 - 30 G. Sonavane, K. Tomoda and K. Makino, *Colloids Surf., B*, 2008, **66**, 274.
 - 31 B. C. H. May, A. T. Fafarman, S. B. Hong, M. Rogers, L. W. Deady and S. B. Prusiner, et al., *Proc. Natl. Acad. Sci. U. S. A.*, 2003, **100**, 3416.
 - 32 H. N. A. Tran, S. Bongarzone, P. Carloni, G. Legname and M. L. Bolognesi, *Bioorg. Med. Chem. Lett.*, 2010, **20**, 1866.
 - 33 C. Ryou, G. Legname, D. Peretz, J. C. Craig, M. A. Baldwin and S. B. Prusiner, *Lab. Invest.*, 2003, **83**, 837.
 - 34 K. Guenther, R. J. Deacon, V. H. Perry and J. N. P. Rawlins, *Eur. J. Neurosci.*, 2001, **14**, 401.
 - 35 G. Dell'Olmo, E. Vannoni, A. L. Vyssotski, M. A. Di Bari, R. Nonno and U. Agrimi, et al., *Eur. J. Neurosci.*, 2002, **16**, 735.
 - 36 G. Giaccone, B. Canciani, G. Puoti, G. Rossi, D. Goffredo and S. Iussich, et al., *Brain Pathol.*, 2000, **10**, 31.
 - 37 H. Fraser and A. G. Dickinson, *J. Comp. Pathol.*, 1968, **78**, 301.